Integration of micro-CT and histology data for vasculature morpho-functional analysis in tissue regeneration

Integration of micro-CT and histology data for vasculature morpho-functional analysis in tissue regeneration

Antonio Palladino[1], Aurelio Salerno[2], Antonio Crasto[1], Carla Lucini[3], Lucianna Maruccio[3], Livia D'Angelo[3], Paolo Antonio Netti[2], Paolo de Girolamo[3], Antonio Cacchioli[4], Chiara Attanasio[2,3], Francesca Ravanetti[4]

(1) Università degli Studi di Napoli Federico II, Dipartimento di Agraria. (2) Istituto Italiano di Tecnologia, Center for Advanced Biomaterials for HealthCare@CRIB. (3) Università degli Studi di Napoli Federico II, Dipartimento di Medicina Veterinaria e Produzioni Animali. (4) Università degli studi di Parma, Dipartimento di Scienze Medico-Veterinarie.

Abstract

The demand for artificial or bioartificial engineered tissues is increasing today in regenerative medicine techniques to replace and restore the physiological function of damaged tissues. Such engineered constructs hold different properties depending on the tissue to be replicated. As for vascularized tissues, complex biocompatible structures, namely scaffolds, play a key role in supporting oxygen and nutrient supply, thus sustaining tissue neoformation and integration with the host. Scaffold architecture significantly impacts its regenerative potential, while preclinical trials are essential to define scaffold-host interactions. In compliance with the 3R principle, there is a clear need to optimize both the procedures to evaluate scaffold performance and the analysis methodology decreasing the number of animals required to gain consistent data. In parallel, current technologies used in preclinical research generate huge amounts of data that need to be elaborated and interpreted correctly. Therefore, we designed this study to evaluate the results of scaffold integration with the host tissue after implantation in a mouse subcutaneous pocket model. We evaluated the angiogenic response developed by the host and the degree of scaffold integration by
using a combined morphometric approach based on both histological and micro-CT analyses. Six- layer scaffolds, made of polycaprolactone (PCL) microspheres, with an ordered structure were produced by thermal sintering. Scaffolds were then implanted in BALB/c mice and retrieved 21 days post-implantation when the animals were deeply anesthetized and perfused with Microfil, a contrast agent for micro-CT. Here, we describe a method to extract quantitative data from micro-CT reconstructions such as (i) total vessel volume; (ii) % of vessel penetration; (iii) distribution of vessel diameters. The general principle of this approach is the refinement of the region of interest (ROI), thus producing a volume of interest (VOI) that matches scaffold volume. This VOI serves as a dataset from which to extract volumetric information. Then VOIs are divided into three identical parts, proximal, median, and distal, to follow the vessel progression into the scaffold, thus obtaining their depth of penetration (DoP). By this methodology, we observed in mean, among the analyzed samples, a vessel invasion for 1,38 mm3 corresponding to the 1,53% of the scaffold volume. We then looked at the diameter distribution being this value a key indicator of vessel maturity, highlighting that 55% of vessels fall into the range from 5,99 µm to 53.99 µm while the remaining 45% are distributed into intervals from 54 to 136 µm. In parallel, to evaluate tissue integration in detail, histological and immunofluorescent analyses were performed to look at vessel distribution and collagen synthesis. Histological results strongly correlate with the micro-CT data providing, however, an overview of the ingrowth tissues. In addition, by immunofluorescent analysis we demonstrate

that newly formed vessels are mature at the considered time point and tissue collagen deposition is widespread within the scaffolds. Collectively, we propose a new method to track vessel formation by using a multi-modal approach posing the basis for: i) the fabrication of novel scaffolds for Tissue Engineering; ii) the integration of detailed information for a wide range of morphological and functional analyses.

Introduction

Tissue engineering (TE) is a multidisciplinary research and clinical field focused on the development and use of bioartificial tissues and organs. Artificial or bioartificial engineered tissues can replace damaged anatomical entities by partially or totally restoring their physiological function (Langer and Vacanti, n.d.). Engineered skin and cartilage were the first tissues used in the clinics (Kremer et al., 2000). Afterwards, TE applications were extended to other tissues such as liver (Ohashi et al., 2005), bone (Salgado et al., 2004), and muscle (Deasy et al., 2004), as well as adipose (Flynn and Woodhouse, 2008) and nervous (Lundborg, 2004) tissues. The potential of TE is not limited to human health, but it comprises veterinary medicine as well. Over the past decade, there has been a growing demand for more sophisticated treatment options for companion animals, including the development of innovative strategies based on the use of stem cells for the treatment of musculoskeletal injuries and chronic diseases (Mavaro et al., 2020; Palladino et al., 2019). On the other hand, some therapeutic approaches based on TE are already part of the clinical practice in equine regenerative medicine with promising results, mainly for the treatment of tendon and cartilage lesions, tendinopathies, and degenerative joint disorders (Sample et al., 2018). Moreover, in veterinary orthopedics, tissue damage is frequently caused by chronic diseases with few satisfactory treatments available (Patruno and Martinello, 2014). In 2020, De Angelis and collaborators published an inspiring study for the creation of cellularized scaffolds using cells of veterinary interest (De Angelis et al., 2020). In this study, chondrocytes were extracted from the metatarsophalangea and metacarpophalangea joints of horses of various ages and breeds. After several culture steps, these cells de-differentiate to stem cell stage, opening up a new potential scenario for the manufacture of scaffolds for the treatment of bone defects in veterinary medicine. Depending on the tissue to replicate, each type of engineered construct displays different properties. In the case of vascularized tissues, we consider complex three-dimensional constructs within which cell survival is strictly related to oxygen concentration, generally limited due to its reduced diffusion, as well as to nutrient supply inside the tissue. For this reason, cell survival and, therefore, the function of the implanted tissue tends to gradually decrease over time (Colton, 1995; Sekiya and Shimizu, 2017). The most common approach in tissue engineering is based on the combined use of scaffolds and cells, and additionally, bioactive molecules to support tissue formation and scaffold
integration with the host tissue (Saleh and Bryant, 2018). Modern approaches aim to guide tissue regeneration using growth factors to simulate physiological conditions. In addition to growth factors, scaffold design plays a critical role in encouraging or limiting the integration with the host tissues, therefore, the development of an effective scaffold must also include its architecture (Rossi et al., 2016). Diloksumpan and colleagues (Diloksumpan et al., 2020) recently created ceramic scaffolds with variable internal architectures, characterized by a gradient of porosity or a constant pore distribution. In order to estimate the construct ability to drive bone regeneration, such constructs were implanted in critical size defect of the iliac tuberosity in Criollo breed horses with an average age of 7 years. After 7 months, the total volume of newly formed bone and the level of scaffold degradation were significantly higher in

the case of constant porosity constructs, according to the comparison between the scaffolds with constant porosity and those with porosity gradient. It is worth noting that scaffolds featured by a porosity gradient showed lower degrees of regeneration and remodeling even in those areas where porosity was similar to that reported for the scaffolds with constant porosity. To quantify the regenerative capability of a certain bioengineered construct in vitro, studies to assess biocompatibility and cell migration throughout the scaffold must first be performed. Following, in vivo characterization is required due to the lack of information provided by the in vitro study in relation to cellular interactions with the host organism. In the context of preclinical studies, multi-parametric evaluation of scaffold interaction with the host tissues is crucial for better defining the characteristics and intrinsic potential of these constructs for their translation into the clinics. Based on the above-mentioned examples, it is clear the need to optimize the procedures for evaluating the performance of the constructs after their explant. This is consistent with the 3R principle, since an improved analysis methodology directly impacts the quality of data also leading to the reduction of the number of animals used in the trial. Current technologies used in preclinical research generate a massive amount of data. As a result, there is a need to elaborate and interpret them correctly to fully exploit their inherent potential. Rather than follow well-established approaches to evaluate scaffold performance used in preclinical trials, such as histological techniques or the most recent micro-computed tomography (micro-CT), it may be beneficial to develop a dedicated workflow to obtain higher-quality data (Palladino et al., 2021).
And it is in this scenario that we designed this study in which we present the results of scaffold implantation in murine hosts evaluating the angiogenic response and, therefore, the integration degree by using a combined morphometric approach based on both histological and micro-CT analyses.

Material and methods

Scaffold preparation

Scaffolds with an ordered structure were produced using the thermal sintering technique. The constructs were made from basic units, or building blocks, made of polycaprolactone (PCL) microspheres with 500 µm mean diameter. The microspheres were assembled and sintered to form a cubic structure with a thickness of 3 mm and a side of 5.5 mm. This fabrication technique consists of several phases. The first step was the manufacture of the PCL microspheres using the oil/water fluidic emulsion technique (Pedram et al., 2021; Salerno et al., 2013). The oil phase consists of a PCL solution (10 % w/v) in dichloromethane (DCM), while the water phase consists of a water solution of Tween 20 (0.1 v/v%) and PVA (0.5 w/v%). The fluidic emulsion was carried out in a custom-made device. The PCL/DCM solution was pumped at 90 µl/min by using a syringe pump (AL300-220, World Precision 152 Instruments Company, Friedberg, Germany) and emulsified by the water solution flowing at 9 ml/min. The droplets of the PCL/DCM solution dropped into a beaker containing 100 ml of Tween 20 (0.1 v/v%) and PVA (0.5 w/v%) water solution and stirred at 190 rpm for three hours to achieve solvent evaporation and microspheres setting. To prepare the microspheres sintered layers with pre-defined cubic-shaped patterns, the microspheres were poured onto patterned polydimethylsiloxane (PDMS) mold, fabricated by soft lithography technique, followed by thermal sintering at 64°C and seven minutes in an oven to create a unique structure forming a monolayer made by microspheres joined together.
Six monolayers of microspheres were aligned and stacked in a PDMS mold followed by solvent

vapors sintering to create an ordered three-dimensional structure having biomechanical properties suitable for in vivo implantation (Salerno et al., 2022).

Scaffold morphology

The morphology of the PCL microspheres scaffolds was assessed by scanning electron microscope (SEM, Ultraplus, Zeiss, Germany) analysis. The scaffolds were gold sputtered using a sputter coater (208HR, Cressington, UK) and SEM analysis was performed at an accelerating voltage of 10 kV.

Scaffold implantation

The six-layer scaffolds were implanted in six female BALB/c mice 6-8 weeks of age (Envigo, Indianapolis, Indiana, US) to test their potential in the preclinical scenario. All animal experiments were performed under the Directive 2010/63/EU (135/2019-PR). Mice were kept under 12:12 hour dark/light cycle with ad libitum access to food and water. Before surgery, the animals were subjected to analgesic therapy with Carprofen at a dose of 4mg/kg administered subcutaneously and then anesthetized via intraperitoneal injection of Ketamine/Medetomidine 100mg/kg+0,25mg/kg. The animals were placed in sternal decubitus, after disinfection with 10% Betadine, a sagittal incision of about 0.5 cm was made behind the shoulder along the median line. The previously sterilized scaffold was then placed inside a 1 cm long subcutaneous pocket, and the incision was sutured with 4/0 silk suture.

Microfil perfusion and explant

At the established endpoint, 21 days post-implantation, mice were deeply anesthetized by intraperitoneal injection of ketamine (75 mg/kg body weight) and xylazine (15 mg/kg body weight). Microfil® (Microfil® MV-122, Flowtech, Carver, Massachusetts, US) was formulated at the viscosity ideal for small vessel filling (3ml:7,5ml:335µl; pigmented compound: diluent: curing agent, respectively) and perfusion was made as previously described (Rossi et al., 2016). At the end of the procedure, perfused animals were carefully coated in aluminium foil and kept at 4°C overnight to enhance curing. The day after, the scaffolds were harvested, fixed in 10% formalin, and stored at 4 °C until micro-CT scanning 24 hours later.

Micro-CT acquisition

Microfil® perfused scaffolds were scanned with a Bruker Skyscan 1172 (Bruker, Billerica, Massachusetts, US). We designed custom-made polymethylmethacrylate (PMMA) holder to reduce the absorbance of the material and isolate the sample from the surrounding background. Explanted scaffolds were placed in these custom-made holders also to obtain the best orientation of the samples, instrumental for the subsequent analyses. Scanning parameters (voltage 40 kV, current 250 µA, power 10 W) were kept constant among samples. The pixel size was set at 5.99 µm to get the best spatial resolution obtainable by the scanner when acquiring such big objects. Images were averaged three times and the rotation step was 0.3 degrees to guarantee a high-quality image in a relatively short time. Data reconstruction was performed via NRecon software by adjusting the alignment and reducing ring artifacts to improve the overall quality of the reconstruction.

Micro-CT measurements

Quantitative data were extracted using CtAN software (Bruker, Billerica, Massachusetts, US). The analyses started with the measurement of both the length and width of the reconstructed samples. Samples measurement are fundamental prerequisites of the proposed methodology. A further significant aspect before starting the evaluations is the adequate scaffold placement in the chamber which must be perpendicular to the x-ray source and then, the manual adjustment of the alignment during reconstruction. These preliminary procedures simplify all the downstream procedures. Then here we describe a method to extract quantitative data from the reconstructions such as: (i) total volume of sample invaded by vessels; (ii) % of vessel

penetration inside the scaffold; (iii) distribution of vessel diameters inside the retrieved samples (Palladino et al., 2021).
The general principle of this approach is the exact refinement of the region of interest (ROI) around the CT reconstruction of the samples. The sum of all the ROIs produces a volume of interest (VOI) that matches the volume of each scaffold. The second part of the approach exploits this VOI as a subset from which volumetric information can be extracted. The last step of the analysis implies the division of the ROIs (and then VOIs) into 3 identical parts, proximal, median, and distal, identified based on the entry zone of most of the vessels. Each of these identical subsets is evaluated to follow vessel progression inside the scaffold and, therefore, it is a representation of the depth of penetration.
In more detail, measurements started by delimiting the range of sections to be analyzed. In this way, only the sections corresponding to the scaffold (approximately 500 sections for each sample) were considered.
The next step was the measurement of the sample and the total ROI drawn around the sample. During this step, ROI dimensions were annotated to be divided later in the pipeline. The identified ROIs were then submitted to CtAN software to gain the results of the volume analysis. Among the different parameters resulting from the analysis, the one indicated as “VOI total volume” measured the volume of the scaffold after ROI cropping. To analyze exclusively the percentage of organ volume covered by vessels, the analysis must be restricted to signals originating from the vasculature. To this aim a threshold value unique for each sample must be identified. This segmentation step was made by a supervised approach. Vessel signals were manually selected with an accurate removal of background signals. We then validated the threshold values by submitting the samples to the “Thresholding” function of CtAN software. This simple procedure, by choosing the function “3D analysis” of CtAN software, enabled the quantitative evaluation of highlighted structures, in our case the vessels. In this step, the report generated by CtAN software included several parameters such as the total volume occupied by vessels (expressed in µm3) but also the percentual distribution of their diameters. To assess to what extent vessels invaded our construct, we used the abovementioned conventional definition of the three scaffold zones, named as proximal, median and distal. To do this, we manipulated the total ROI. Starting from the whole ROI we identify its dimensions, in particular the width. This parameter (expressed in pixels or µm) was dived by 3 to highlight a subset of µVOIs corresponding to only one part of the scaffold (proximal, median, or distal). This subset was analyzed as the total VOI to extract volumetric parameters. This operation was iterated by each of the 3 ROIs and the corresponding values annotated. Out of all parameters, the “Object volume” is the key one to be considered to evaluate vessel penetration. Using this variable, we estimated the percentage of vascularization of each zone through the
following formula: % of vessel of ZONE x = Object volume ZONE x /Object Volume Whole ROI.
We evaluated the diameter distribution as a functional indicator of the newly formed vascular network in combination with the analysis of vessel penetration inside the scaffold. The built-in features of the “3D analysis” of CtAN software generated a report from which the percentage of objects (in our case, vessels) that fall within a certain diameter was extracted. The following results were then analyzed, and the diameters divided into 12 µm intervals ranging from 5.99 µm to 137.98 µm. Figure 1 illustrates the diagram recapitulating micro-CT workflow.

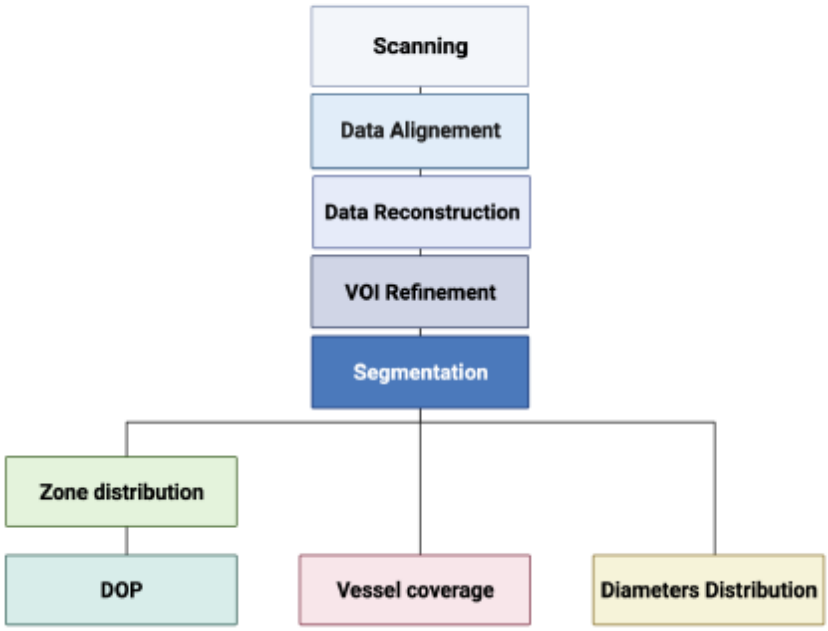

Figure 1 Micro-CT workflow. The flowchart summarizes the single passages required for the micro-CT analysis described in the text.

Histology

After micro-CT analysis, the harvested tissues including the scaffolds were dehydrated in increasing alcohol concentrations, clarified in xylene, and paraffin embedded. The embedding orientation was micro-CT guided. Sections 5 µm thick, parallel to the scaffold horizontal plane, were obtained using a rotary microtome (Slee Cut 6062, Slee Medical, Mainz, Germany). Sections were stained with hematoxylin–eosin (H&E). Whole slide images (WSI) were acquired using NanoZoomer S60 slide scanner (Hamamatsu Photonics K.K., Hamamatsu City, Japan).

Immunofluorescence

Immunofluorescent (IF) reactions were performed as previously described (Mascadri et al., 2021) on paraffin embedded sections to detect newly formed vessel network within the scaffold. Briefly, paraffin embedded sections were deparaffinized, rehydrated, and then antigen retrieved (in a 10 mM citrate buffer at a boiling point). After a cooling step, the slides were rinsed in a washing buffer and then immersed in a blocking buffer (0.3 M glycine, 5% bovine serum albumin in PBS; Sigma- Aldrich, St Louis, Missouri, US) at room temperature. Sections were incubated over night at 4°C with primary antibody (Dako/Agilent anti-αSMA: 0.14 µg/ml, 1A4/M0851; Abcam anti-Collagen type I: 2.5 µg/ml, ab88147). The reaction was revealed by 1 hour RT incubation with specific secondary antibodies (Jackson ImmunoResearch, goat anti-mouse IgG, subclass 2a specific, Rhodamine Red – X (RRX), dil. 1:200, 115-295-206; Jackson ImmunoResearch, goat anti-mouse IgG, subclass 3 specific, Alexa Fluor 647 conjugate: dil. 1:500, 115-605-209). Finally, the nuclei were counterstained with DAPI (Invitrogen). For negative control the primary antibody was omitted, and tissues were incubated in 10 mM phosphate buffer or, alternatively, with unlabeled rabbit IgG nonimmune isotype control (2009-1; Alpha Diagnostic International) used at the same concentration as the selective antibody. Fluorescent Whole Slide Imaging were acquired using NanoZoomer S60 slide scanner (Hamamatsu Photonics K.K., Hamamatsu City, Japan).

Vessel histomorphometry

The vascular network formation into the scaffolds was histologically evaluated within three different scaffold compartments: proximal, median, and distal. For each compartment three randomly selected ROIs (448 x 780 μm) were used to identify and count the vessels. Data are express as mean ± SD.
Statistical analysis was performed using t-test using GraphPad Prism (v 9.0, GraphPad Software Inc). A value of $P < 0.05$ was considered statistically significant.

Results

In vivo study
The implanted scaffolds were retrieved and analyzed after 21 days via micro-CT. Mice were perfused with Microfil® before the explant to highlight the vessels that penetrated the scaffolds. With our protocol, we obtained data from the micro-CT scans. The analysis of this dataset allowed us to measure the volume occupied by the blood vessels inside the scaffold, as well as their distribution and diameter.
In our procedure, we first evaluated the dimension of the scaffold after retrieval. This is instrumental to both checking scaffold dimension after implantation and accurately "double-checking" total volumes. In More detail, the dimensions were 5,4x5,4x2,7 mm, therefore, slightly reduced in comparison to those recorded before implantation: 5,5x5,5x3 mm.
The next step of the analysis was made possible by modeling the ROI around the volume of the scaffold. In this way, we estimated that the scaffolds occupied on average a volume of 86,44 mm3 (±6,789 mm3).

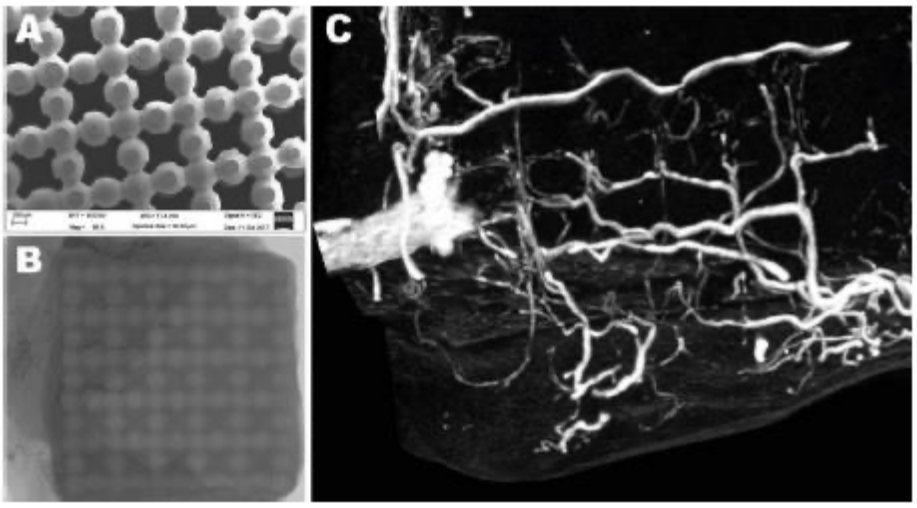

Figure 2 Scaffold measurement setting. In A it is reported a SEM image of the scaffold before implantation. In B it is appreciable the whole scaffold after micro-CT scanning and reconstruction. In C it is imaged a particular of the perfused vessels, highlighted by the proposed protocol, entering the scaffold.

Vessel volume measurement
Then, for each explant, we assessed the vascularization parameters previously mentioned. All the values described below were normalized by vessel volume recorded in the host at the implantation
site, detected in the skin around the implantation area. The percentage of vascularization was the first value evaluated. The percentage of vascularized volume in the first specimen (Sample 1) was 0.09%. This percentage fills up 0.0725 mm3 of the scaffold volume. The second scaffold investigated (Sample 2) showed a percentage increase of up to 1.33%.

This value is equivalent to 1,103 mm3. The last scaffold studied (Sample 3) contained the 3,19% of vessels corresponding to 2,978 mm3.

Vessel distribution analysis

We defined the depth of penetration of the vessels by dividing the scaffold into three identical zones. These areas were identified on a constant basis by analyzing the sample and evaluating the blood vessel entry point. Based on this classification, we defined the 3 zones as: proximal, median, and distal. Each zone had an approximate length of 1733 µm. Therefore, the proximal one lay in a range of 0-1733 µm, the median to 1733-3466 µm and the distal one from 3466-5200 µm.

The analysis of the first sample revealed that 63,50 % of vessel volume was in the proximal zone, while 16,71 % and 19,79 % were in the median and distal zones, respectively. The distribution of vessel volume in the second sample was as follows: 58,84 % is in the proximal zone, 24,01 % is in the median zone, and 17,15 % is in the distal one.

The evaluation of vessel volume of the third sample revealed the following distribution: 34,71% in the proximal portion, 32,65% in the median and 32,63% in the distal one.

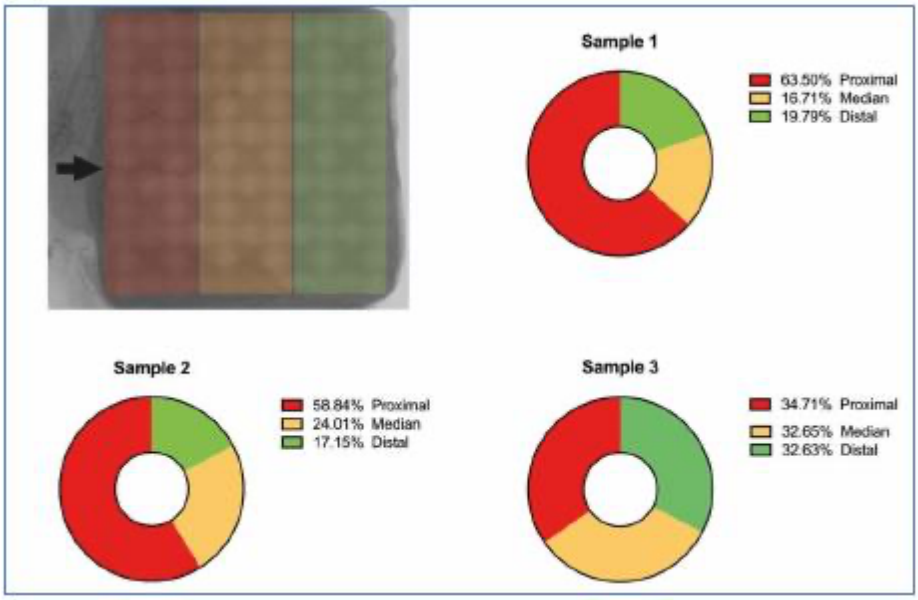

Figure 3 Vessel distribution measurement. The figure illustrates scaffold division to assess vessel depth of penetration within the scaffold. In the diagrams are listed the results relative to each sample divided by the three identified zones.

Diameter distribution

Along with vessel distribution, another important parameter to consider is diameter distribution being this value a key indicator of vessel maturity also providing functional data. The diameters were grouped as intervals of 12 µm ranging from 5,99 to 137,98 µm. Analyses of sample diameters (summarized in Figure 4) revealed that more than half of the total blood vessels (55%) fell into the range 5,99-53.99 µm that covers the first 4 intervals with respectively 15, 23,17 and 14 %. The remaining 45% of vessels are distributed into intervals from 53.99 to 137.97µm.

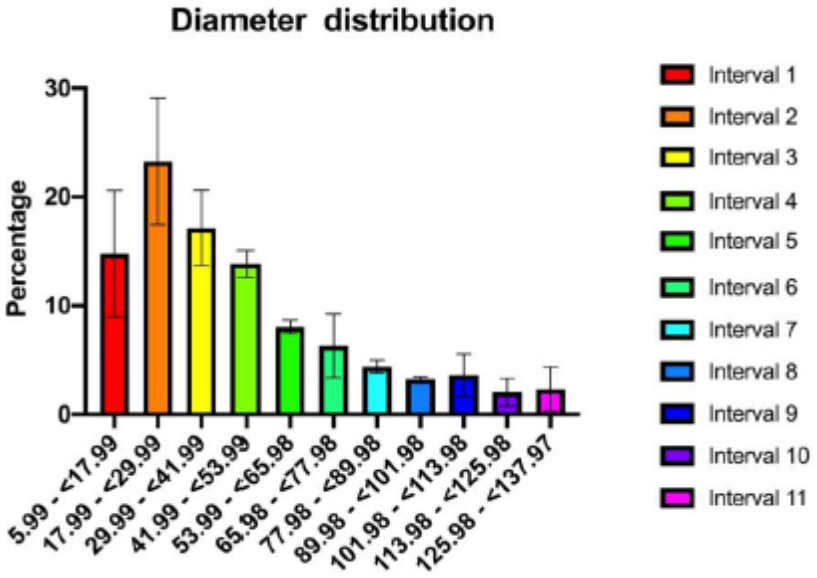

Figure 4 Diameter distribution analysis. The diagram represents vessel diameter distribution inside the scaffolds. For the analysis were identified 11 intervals of 12 µm range. Each interval corresponds to a relative percentage. Results indicate that 55% of vessel diameters falls in the first 4 intervals (from 5,99 to 53,99 µm).

Vessel morphology assessment

The histological analysis of the scaffolds revealed the complete ingrowth of fibrous connective tissue into the scaffold (Figure 5). The Microfil® perfused vessels were histologically detectable in brightfield microscopy on H-E staining. Vessels within the scaffold structure appeared as dark brown dots (Figure 5), then the vessel endothelium microstructure was confirmed by microscopic analysis. The vessel count was performed on immunofluorescence staining of α-SMA (Figure 5 a-f). The vessel counts within the ROIs showed a higher number of vessels in the proximal portion (Figure 5 g). The vessel counts in histology confirmed the micro-CT 3D detection, showing a decreasing trend of vessel formation going from proximal to median and distal scaffold partitions. Regarding the fibrotic tissue ingrowth into the scaffold, cells within the interstitial space between the pores, synthesized collagen-based ECM as confirmed by Collagen immunofluorescence detection.

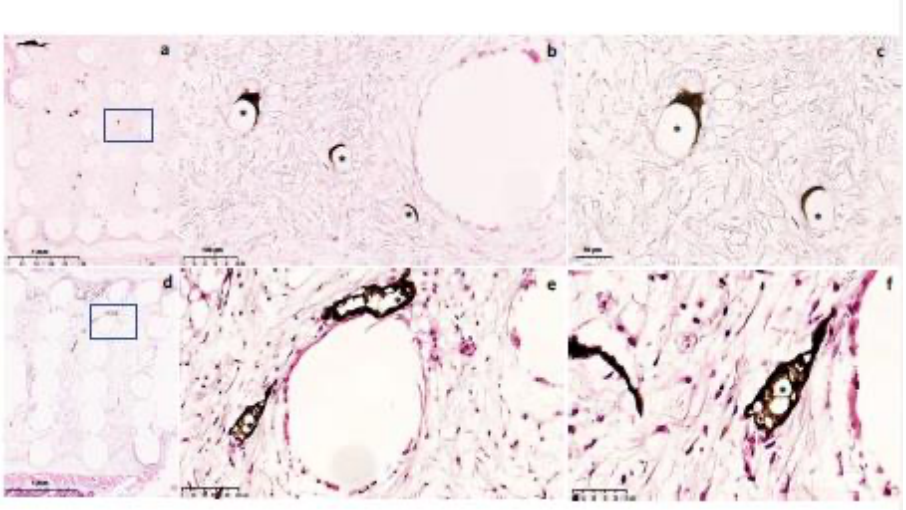

Figure 5 Histological sections of the implanted scaffolds stained with Hematoxylin-Eosin. Newly formed vessels perfused with Microfil® (asterisk) were clearly detectable on the tissue

ingrowth into the scaffold. Sequential increasing magnification: a-d (1X); b-e (10X); c-f (20X). Sample 1(a,b,c); Sample 2 (d,e,f).

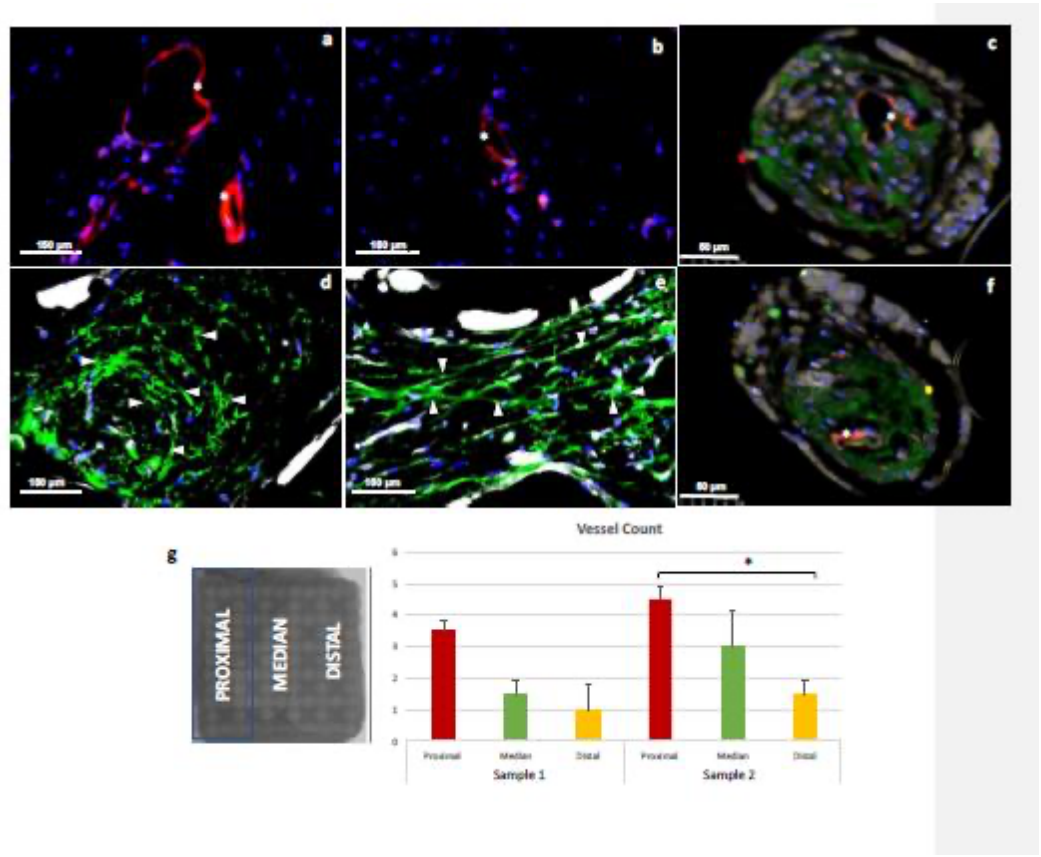

Figure 6 Immunofluorescence analysis. Representative microphotographs of the immunofluorescence staining for αSMA (a,b) showing the tunica media of vessel (asterisk) and for Collagen type I (d,e) showing the connective ingrowth tissue (head arrow). Merge of channels in c and f. Sample 1(a,d,c); Sample 2 (b,e,f).
Histograms represent means± SD of vessel count for different scaffold compartments. The asterisk above the bars indicates significant difference in the comparison among compartments (*P < 0.05).

Discussion

Science is based on innovation and anatomical science is also evolving every day. Innovation runs in parallel with the development of new instruments and protocol refinement. Certainly, micro-CT introduction in anatomy research caused an outbreak in the knowledge in terms of new discoveries and reversion of erroneous conceptions.
As an example, micro-CT scansion of feline hearts by Matos and colleagues (Matos 2020) allowed to characterize and measure fibrotic mass in hypertrophic cardiomyopathy. By means of micro-CT scans the authors were able to detect different hallmarks of the pathology with the same accuracy of common histopathology sample processing more quickly and efficiently suggesting that micro-CT may be used routinely for post-mortem analyses to discover hypertrophic cardiomyopathy.

With the same approach Doost and colleagues (Doost et al., 2020), after dissection and weight, scanned iodine-perfused murine hearts to determine left ventricle mass. The approach was highly reliable and showed a strong correlation to the measurements made by dissection, however, it holds the direct advantage of being nondestructive and very accurate to extract quantitative data for translational studies.
Also, normal anatomic investigations in largely studied tissues such as liver benefit of micro-CT paving the way to new discoveries. In a recent paper (Kline et al., 2014) the authors studied in detail rat liver perfusion by injection of a radiopaque agent providing the first evidence of shunts occurring between hepatic artery and portal vein branches.
In a recent work (McManus et al., 2012) serial micro-CT scans of temporal bones have been performed to better define the precise anatomy of the posterior canaliculus housing the chorda tympani providing evidence useful in otologic surgery since the iatrogenic injury of the nerve is one of the most frequent complications during surgery. In a study on the same anatomical district (Li et al., 2018) Li and colleagues employed micro-CT scanning to study human cochlear aqueduct. The exact anatomy of this bony canal linking the scala tympani and the cranium, is still not well described. Before this study the canal was observed only by histological sections, therefore, the exact path through the temporal bone, and consequently, its putative function was still poorly understood. Also in this case, this evicence represents a new benchmark to assess possible anatomical anomalies and follow the structure modification during aging.
Despite being instrumental for new discoveries and detailed structure characterization, micro-CT analysis cannot entirely replace histological techniques which provide fundamental information concerning tissue morphology.
Our work was devoted to developing an integrated approach to evaluate how an advanced scaffold integrates into murine hosts after subcutaneous pocket implantation. This approach ensures a detailed characterization of the angiogenic response and the tissue neoformation throughout the scaffold.
The preliminary micro-CT analysis performed before considering vessel neoformation, provides valuable data concerning scaffold structure.
The novel design of the scaffold is characterized by a high porosity (Salerno et al., 2022) required to increase tissue ingrowth to facilitate an adequate transport of oxygen and nutrients to efficiently remove waste products (De Mulder et al., 2013). This architecture could result in faster resorption which reduces the levels of acidic compound release, thus promoting tissue regeneration (Van Minnen et al., 2005). It is essential to point out that we have not focused our analysis on the immunological response of the host, however, from a macroscopic analysis and through the methodology applied we can sustain that the scaffold did not create an appreciable adverse response after implantation. This is in line with the expected high biocompatibility of polycaprolactone scaffolds (F Lam et al., 2008). Further. our preliminary measurements indicate the presence of a slight reduction in scaffold dimensions after implantation (5,5x5,5x3 mm vs 5,4x5,4x2,7 mm). This finding is attributable to a dorsoventral compression operated by host tissues rather than PCL degradation that should occur after the 21-day endpoint. It is worth to note that the structure was maintained in all the samples analyzed indicating an overall robustness of the scaffold design and PCL microsphere disposition. The main outcome of this is that, thanks to micro-CT analysis it is possible to perform a wide range of measurements to determine scaffold structural performances after in vivo implantation.
Regarding micro-CT analysis of vascular invasion our approach considered three main aspects: i) the percentage of scaffold volume invaded by vessels; ii) the hierarchy featuring

vessel distribution within the scaffold; iii) the distribution of diameters as an indication of vascular network maturity. The volume of the vessels detected within the scaffold is an essential indicator of scaffold performance after implantation, since only a highly biocompatible construct could create the right spatial and biochemical conditions to support vascular growth during regeneration. The method we designed requires the preliminary step of VOI refinement by an iterative ROI drawing approach. This prerequisite refines scanning volume to the scaffold only. This passage must be supervised by the operator and has the advantage to be finely checked avoiding possible volume estimation mistakes made by computer-aided approaches. Prerequisite to vessel quantification is a
segmentation passage. The signals relative to vessels contrasted by Microfil® are identified and isolated from the background. As the previous one, also this passage is under the complete control of the operator and allows to adapt segmentation conditions to each scan. These preliminary steps result in a more direct sample analysis and directly usable values compared to the standard procedure.
In our study the presence of signal conducible to the contrast agents within the ingrowth vessels revealed their complete perfusion implying a fully functional connection with host vasculature at the implantation site.
The result identifies different trends of vascular growth within the scaffold, with percentages ranging from 0.09 % (0.0725 mm3) of the first sample to the 3,19% (2,978 mm3) of the third one. In relation to the integration of the host tissue and the support of the onset vascular network within the scaffold, the data gained in this study seem to be encouraging in comparison to those resulting from the analysis of kidney vasculature (about 8%) reported in a previous work of our group (Palladino et al., 2021). A further encouraging aspect is the potential of the described approach in detecting a wide range of vessel volumes which is especially useful to test scaffold performance in regenerative medicine trials.
To score vessel depth of penetration within the construct, scaffold volume was divided into three identical zones (with an approximate length of 1733 μm) defined as: proximal, median, and distal. Sample analysis demonstrates two different trends: in the first two samples there was a prominent vessel presence in the proximal zone with a decreasing percentage toward the distal area while in the last sample a more homogeneous distribution was detected among all the zones. These findings could suggest a monovalent entrance of the vessels in the first case in contrast to a multidirectional and more distributed vessel entrance in the last sample. Since samples share the design, this feature is more likely to be attributable to a slight difference in host regional vascularization at the implantation site rather than to an inadequate scaffold design. This hypothesis is supported by the evidence that in all the considered samples vessel ingrowth was noted not only on the scaffold surface but was also detectable in the inner areas of the construct.
The last parameter considered was vessel diameters which is instrumental to assess vascular network maturity and evaluate vessel size from a functional standpoint. To assess diameter distribution Microfil® signals were subdivided as intervals ranging from 5,99 to 137,98 μm grouped as intervals of 12 μm. The starting value of 5,99 μm was the minimum voxel chosen according to instrument resolution power and very close to the smallest capillary detected in humans which measures 5 μm (Arakawa et al., 2020). The results indicated that more than half of the total vessel diameters (55%) fall into the interval ranging from 5,99 μm to 53.99 μm, while the remaining part of vessels were distributed in larger intervals ranging from 53.99 to 137.97μm. This evidence is in line with previous observations (BURTON, 1954; O'Connor et al., 2022) and indicate that newly formed vessels fall in the range of functionally mature vessels (capillaries, arterioles, and venules). Also, scanning resolution is a key parameter of the

analysis, our choice was mainly conducible to the best achievable by our instrument, but we are confident that applying this methodology with an increased resolution may lead to more accurate results.

Preclinical testing is crucial to proceed from bench to bedside and prerequisite to this translation involves a careful evaluation of the implanted scaffold which includes to what extent it is effective in supporting angiogenesis, how well the construct integrates with the host tissue and how the host responds to it (Hopkins et al., 2015). Not all these issues can be approached through micro-CT, therefore, they must be afforded using histological methods.

To fulfill this need in our study we associated to a non-destructive micro-CT analysis a subsequent histological and immunofluorescent one.

H-E staining evidenced a full invasion of host tissue within the construct. Tissue formation into the scaffold is a direct consequence of microenvironment, depending, therefore, on structure design (Wang et al., 2019). According to our result the H-E staining confirmed a homogeneous tissue distribution, thus providing further evidence about the correct PCL microsphere spatial disposition.

It is interesting to note how histology provides an additional description on how vessels are distributed across the newformed tissue. This was possible thanks to the presence of dark spots visible into the vessel lumen, a feature directly conducible to Microfil® perfusion. This characteristic could be exploited to provide a correlative analysis in respect to micro-CT regarding vessel distribution. However, to perform a correlative count we evaluate, via immunofluorescence analysis, the fluorescent signals relative to well-known markers of endothelial cells, in particular α- SMA signal was evidenced in pericytes and vascular smooth muscle cells surrounding the endothelial layer (Manetti et al., n.d.) representing, therefore, a marker of mature blood vessels. The number of vessels, in scaffold oriented and sectioned based on micro-CT data, evidenced a high level of vessel invasion in the proximal region of the scaffold with a progressive decrease toward the distal part. This finding strongly correlates and confirms those obtained by micro-CT analysis. This step is crucial not only to confirm 3D data, but also to obtain qualitative information about newly formed vessels as well as to assess vascular network maturity and functionality. Framed in this context the inclusion of specific markers could contribute to add knowledge about neo angiogenesis occurring within a scaffold.

By HE staining we demonstrated a complete invasion of connective tissue in the hollow cavities of the scaffold, and, to further explore ECM composition, we performed immunofluorescent evaluation of Collagen-I expression. Collagen-I is a member of the fibril forming family of collagens, present in a large percentage of the ECM in the body and is a constituent of tissues undergoing angiogenesis (Rhodes and Simons, 2007). Mutants in Collagen-1 are lethal and are characterized by an aberrant fragility of blood vessels (Löhler et al., 1984). Showing the presence of an organized matrix of Collagen-1 fibrils we indicated the onset of a mature environment able to sustain vessel growth and stability.

In any case, by choosing specific antibodies, immunofluorescence can be instrumental to assess ECM composition.

To sum it up, in the present work we illustrated an integrated approach to gain multiparametric quantitative data to track the in vivo performance of a biocompatible scaffold implanted in a murine host. Such approach may be crucial in evidencing and quantifying hallmarks of regenerative processes, such as neoangiogenesis and new tissue formation. However, this methodology has a broad range of applications. Studies of developmental biology and deep morphometric characterization of anatomical structures could benefit from this analysis pipeline due to its modular design which enables to adapt it to study different kind of tissues.

Bibliography

Arakawa, C., Gunnarsson, C., Howard, C., Bernabeu, M., Phong, K., Yang, E., DeForest, C.A., Smith, J.D., Zheng, Y., 2020. Biophysical and biomolecular interactions of malaria-infected erythrocytes in engineered human capillaries. Sci. Adv. 6, 1–10. https://doi.org/10.1126/sciadv.aay7243

BURTON, A.C., 1954. Relation of structure to function of the tissues of the wall of blood vessels. Physiol. Rev. 34, 619–642. https://doi.org/10.1152/physrev.1954.34.4.619

Colton, C.K., 1995. Implantable Biohybrid Artificial Organs. Cell Transplant. 4, 415–436. https://doi.org/10.1177/096368979500400413

De Angelis, E., Cacchioli, A., Ravanetti, F., Bileti, R., Cavalli, V., Martelli, P., Borghetti, P., 2020. Gene expression markers in horse articular chondrocytes: Chondrogenic differentiaton IN VITRO depends on the proliferative potential and ageing. Implication for tissue engineering of cartilage. Res. Vet. Sci. 128, 107–117. https://doi.org/10.1016/j.rvsc.2019.10.024

De Mulder, E.L.W., Hannink, G., Verdonschot, N., Buma, P., 2013. Effect of polyurethane scaffold architecture on ingrowth speed and collagen orientation in a subcutaneous rat pocket model. Biomed. Mater. https://doi.org/10.1088/1748-6041/8/2/025004

Deasy, B.M., Li, Y., Huard, J., 2004. Tissue engineering with muscle-derived stem cells. Curr. Opin. Biotechnol. 15, 419–423. https://doi.org/10.1016/j.copbio.2004.08.004

Diloksumpan, Paweena, Vindas Bolaños, R., Cokelaere, Stefan, Pouran, B., de Grauw, Janny, van Rijen, M., van Weeren, René, Levato, Riccardo, Malda, Jos, Diloksumpan, P, Cokelaere, S, de Grauw, J, van Weeren, R, Levato, R, Malda, J, 2020. Orthotopic Bone Regeneration within 3D Printed Bioceramic Scaffolds with Region-Dependent Porosity Gradients in an Equine Model. https://doi.org/10.1002/adhm.201901807

Doost, A., Rangel, A., Nguyen, Q., Morahan, G., Arnolda, L., 2020. Micro-CT scan with virtual dissection of left ventricle is a non-destructive, reproducible alternative to dissection and weighing for left ventricular size. Sci. Rep. 10, 1–9. https://doi.org/10.1038/s41598-020- 70734-3

F Lam, C.X., Hutmacher, D.W., Schantz, J.-T., Ann Woodruff, M., Hin Teoh, S., 2008. Evaluation of polycaprolactone scaffold degradation for 6 months in vitro and in vivo. https://doi.org/10.1002/jbm.a.32052

Flynn, L., Woodhouse, K.A., 2008. Adipose tissue engineering with cells in engineered matrices. https://doi.org/10.4161/org.4.4.7082

Hopkins, T.M., Heilman, A.M., Liggett, J.A., LaSance, K., Little, K.J., Hom, D.B., Minteer, D.M., Marra, K.G., Pixley, S.K., Professor, A., 2015. Combining Micro-Computed Tomography with Histology to Analyze Biomedical Implants for Peripheral Nerve Repair Corresponding Author and site of work: HHS Public Access. J Neurosci Methods 255, 122–130. https://doi.org/10.1016/j.jneumeth.2015.08.016

Kline, T.L., Knudsen, B.E., Anderson, J.L., Vercnocke, A.J., Jorgensen, S.M., Ritman, E.L., 2014. Anatomy of hepatic arteriolo-portal venular shunts evaluated by 3D micro-CT imaging. J. Anat. https://doi.org/10.1111/joa.12178

Kremer, M., Lang, E., Berger, A., 2000. Evaluation of dermal-epidermal skin equivalents ('composite-skin') of human keratinocytes in a collagen-glycosaminoglycan matrix (Integra(TM) artificial skin). Br. J. Plast. Surg. 53, 459–465. https://doi.org/10.1054/bjps.2000.3368

Langer, R., Vacanti, J.P., n.d. Tissue Engineering.

Li, Z., Shi, D., Li, H., Tan, S., Liu, Y., Qi, C., Tang, A., 2018. Micro-CT study of the human

cochlear aqueduct. Surg. Radiol. Anat. https://doi.org/10.1007/s00276-018-2020-6 Löhler, J., Timpl, R., Jaenisch, R., 1984. Embryonic lethal mutation in mouse collagen I gene causes rupture of blood vessels and is associated with erythropoietic and mesenchymal cell death. Cell 38, 597–607. https://doi.org/10.1016/0092-8674(84)90514-2 Lundborg, G., 2004. Alternatives to Autologous Nerve Grafts. Handchirurgie Mikrochirurgie Plast.
Chir. 36, 1–7. https://doi.org/10.1055/s-2004-820870 Manetti, M., Romano, E., Rosa, I., Guiducci, S., Bellando-Randone, S., De Paulis, A., Ibba-Manneschi, L., Matucci-Cerinic, M., n.d. Endothelial-to-mesenchymal transition contributes to endothelial dysfunction and dermal fibrosis in systemic sclerosis. https://doi.org/10.1136/annrheumdis-2016-210229
Mascadri, F., Ciccimarra, R., Bolognesi, M.M., Stellari, F., Ravanetti, F., Cattoretti, G., 2021. Background-free Detection of Mouse Antibodies on Mouse Tissue by Anti-isotype Secondary Antibodies. J. Histochem. Cytochem. https://doi.org/10.1369/00221554211033239
Mavaro, I., De Felice, E., Palladino, A., Livia D'angelo, |, De Girolamo, P., Chiara Attanasio, |, Attanasio, C., Angelo, L.D.', 2020. Anatomical templates for tissue (re)generation and beyond. https://doi.org/10.1002/bit.27533
McManus, L.J., Dawes, P.J.D., Stringer, M.D., 2012. Surgical anatomy of the chorda tympani: A micro-CT study. Surg. Radiol. Anat. 34, 513–518. https://doi.org/10.1007/s00276-012-0941-z
O'Connor, C., Brady, E., Zheng, Y., Moore, E., Stevens, K.R., 2022. Engineering the multiscale complexity of vascular networks. Nat. Rev. Mater. https://doi.org/10.1038/s41578-022-00447-8
Ohashi, K., Waugh, J.M., Dake, M.D., Yokoyama, T., Kuge, H., Nakajima, Y., Yamanouchi, M., Naka, H., Yoshioka, A., Kay, M.A., 2005. Liver tissue engineering at extrahepatic sites in mice as a potential new therapy for genetic liver diseases. Hepatology. https://doi.org/10.1002/hep.20484
Palladino, A., Mavaro, I., Pizzoleo, C., Felice, E. De, Lucini, C., de Girolamo, P., Netti, P.A., Attanasio, C., 2019. Induced Pluripotent Stem Cells as Vasculature Forming Entities. J. Clin.Med. https://doi.org/10.3390/jcm8111782
Palladino, A., Pizzoleo, C., Mavaro, I., Lucini, C., D'Angelo, L., de Girolamo, P., Attanasio, C., 2021. A combined morphometric approach to feature mouse kidney vasculature. Ann. Anat. 237. https://doi.org/10.1016/j.aanat.2021.151727
Patruno, M., Martinello, T., 2014. Treatments of the injured tendons in Veterinary Medicine: From scaffolds to adult stem cells. Histol. Histopathol. 29, 417–422. https://doi.org/10.14670/HH-29.10.417
Pedram, P., Mazio, C., Imparato, G., Netti, P.A., Salerno, A., 2021. Bioinspired Design of Novel Microscaffolds for Fibroblast Guidance toward in Vitro Tissue Building. ACS Appl. Mater. Interfaces 13, 9589–9603. https://doi.org/10.1021/acsami.0c20687
Rhodes, J.M., Simons, M., 2007. The extracellular matrix and blood vessel formation: Not just a scaffold: Angiogenesis Review Series. J. Cell. Mol. Med. 11, 176–205. https://doi.org/10.1111/j.1582-4934.2007.00031.x
Rossi, L., Attanasio, C., Vilardi, E., De Gregorio, M., Netti, P.A., 2016. Vasculogenic potential evaluation of bottom-up, PCL scaffolds guiding early angiogenesis in tissue regeneration. J. Mater. Sci. Mater. Med. 27, 1–11. https://doi.org/10.1007/s10856-016-5720-7
Saleh, L.S., Bryant, S.J., 2018. The host response in tissue engineering: Crosstalk between immune cells and cell-laden scaffolds. Curr. Opin. Biomed. Eng. 6, 58–65. https://doi.org/10.1016/j.cobme.2018.03.006
Salerno, A., Levato, R., Mateos-Timoneda, M.A., Engel, E., Netti, P.A., Planell, J.A., 2013.

Modular polylactic acid microparticle-based scaffolds prepared via microfluidic emulsion/solvent displacement process: Fabrication, characterization, and in vitro mesenchymal stem cells interaction study. J. Biomed. Mater. Res. - Part A 101 A, 720–732. https://doi.org/10.1002/jbm.a.34374
Salerno, A., Palladino, A., Pizzoleo, C., Attanasio, C., Netti, P.A., 2022. Computer-aided patterning of PCL microspheres to build modular scaffolds featuring improved strength and neovascularized tissue integration. Biofabrication 14. https://doi.org/10.1088/1758-5090/ac7ad8
Salgado, A.J., Coutinho, O.P., Reis, R.L., 2004. Bone tissue engineering: State of the art and future trends. Macromol. Biosci. 4, 743–765. https://doi.org/10.1002/mabi.200400026
Sample, S.J., Racette, M.A., Hans, E.C., Volstad, N.J., Schaefer, S.L., Bleedorn, J.A., Little, J.P., Waller, K.R., Hao, Z., Block, W.F., Muir, P., 2018. Use of a platelet-rich plasma-collagen scaffold as a bioenhanced repair treatment for management of partial cruciate ligament rupture in dogs. https://doi.org/10.1371/journal.pone.0197204
Sekiya, S., Shimizu, T., 2017. Introduction of vasculature in engineered three-dimensional tissue. Inflamm. Regen. 37, 1–8. https://doi.org/10.1186/s41232-017-0055-4
Van Minnen, B., Stegenga, B., Van Leeuwen, M.B.M., Van Kooten, T.G., Bos, R.R.M., 2005. A long-term in vitro biocompatibility study of a biodegradable polyurethane and its degradation products. https://doi.org/10.1002/jbm.a.30531
Wang, K., Lin, R.Z., Melero-Martin, J.M., 2019. Bioengineering human vascular networks: trends and directions in endothelial and perivascular cell sources. Cell. Mol. Life Sci. 76, 421–439. https://doi.org/10.1007/s00018-018-2939-0

Declaration of interests

☒ The authors declare that they have no known competing financial interests or personal relationships that could have appeared to influence the work reported in this paper.